ANALYSIS OF EFFECTS OF MANUAL THERAPY ON MUSCULAR MECHANICS USING FINITE ELEMENT MODELING

by

Selen Ersoy

B.Sc., in Physics, Boğaziçi University, 2007

Submitted to the Institute of Biomedical Engineering
in partial fulfillment of the requirements
for the degree of
Master of Science
in
Biomedical Science

Boğaziçi University
2010

ACKNOWLEDGMENTS

First and foremost, I would like to thank my thesis advisor, Assoc. Prof. Dr. Can A. Yücesoy, for his guidance throughout my study, and also for his tolerance. Furthermore, I would like to thank my thesis examining committee Prof. Dr. Ahmet Ademoğlu and Assist. Prof. Dr. Necla Birgül İyison for their valuable comments and recommendations.

I would like to thank my friends in Biomechanics Laboratory Filiz Ateş, Emre Arıkan and Ahu Türkoğlu for their helpfulness, advice and valuable time.

Finally, I would like to express my gratitude to my family, especially to my mother, for their love, encouragement, patience and support that made everything possible. I dedicate this dissertation to my family.

ABSTRACT

ANALYSIS OF EFFECTS OF MANUAL THERAPY ON MUSCULAR MECHANICS USING FINITE ELEMENT MODELING

In this present study, the specific goal was to evaluate the mechanical effects of manual therapy quantitatively. Physiotherapists primarily aim for increasing the range of motion of restricted joints during treatment, therefore lengthening of the target muscle was highly important for this study. Simulation of therapeutic loading was applied at three different locations (Location P, I, and D) for single loading cases and at two different locations (Location P-I and Location I-D) for multiple loading cases on EDL muscle model of rat with extramuscular connections. Nodal strain percentage changes of Case P, Case I, and Case D and Case P, Case P-I and Case I-D loading cases were compared. Loading the muscle model at a proximal location yields more pronounced percentage changes for both fiber and cross-fiber direction nodal strain and for strain distributions. These effects were shown to be more substantial for compressive loading compared to loading in tension. Our results also suggest that increasing the number of loading locations does not provide any notable improvement in the intended effects of manual therapy. Our results should be tested in clinical environment to have a scientific basis of the effects of therapeutic loading of muscles.

Keywords: Manual Therapy, Muscle Mechaniccs, Finite Element Modeling, EDL Muscle, Graston Technique.

ÖZET

EL REHABİLİTASYONUNUN KAS MEKANİĞİ ÜZERİNDEKİ ETKİLERİNİN SONLU ELEMANLAR ANALİZİ İLE İNCELENMESİ

Çalışmanın temel amacı, el rehabilitasyonunun kas mekaniği üzerindeki etkilerinin sonlu elemanlar analizi ile incelenmesidir. Fizyoterapistler, el rehabilitasyonu tedavisinde kuvvet uygularken, öncelikli olarak eklem hareket aralığını arttırmaya çalışmaktadırlar; dolayısıyla tedavinin uygulandığı kas ya da kas grubunun uzama durumu büyük önem taşır. Bu çalışmadaki ekstramüsküler bağlantılı sıçan EDL kas modelinde, tekli yükleme durumunda üç ayrı lokasyonda (Koşul P, I ve D)çoklu yükleme durumunda ise iki ayrı lokasyonda (Koşul P-I ve Koşul I-D) olmak üzere beş farklı koşul oluşturulmuştur. Model noktalarındaki şekil değiştirme yüzde değişimleri, ilk önce tekli yükleme koşulları arasında daha sonra Koşul P, Koşul P-I ve Koşul I-D arasında kıyaslanmıştır. Kası proksimal bir bölgeden yüklemenin fiber ve karşı-fiber yönündeki gerilim yüzdelerindeki değişimlerine katkısı daha fazla olmaktadır. Bu etkilerin, itme kuvveti koşullarında çekme kuvvetinin uygulandığı koşullardan daha belirgin olduğu gösterilmiştir. Aynı zamanda yükleme lokasyonunun sayısını arttırmanın istenen sonuçlarda belirgin bir artışa yol açmadığı gösterilmiştir. Sonuçlarımız, kası tedavi edici yüklemenin bilimsel temellere dayanabilmesi için klinik ortamda test edilmesinin gerekliliğini göstermiştir.

Anahtar Sözcükler: El Rehabilitasyonu, Kas Mekaniği, Sonlu Elemanlar Analizi, EDL Kası, Graston Tekniği.

TABLE OF CONTENTS

LIST OF FIGURES

LIST OF TABLES

LIST OF SYMBOLS

a_{ij}	Description of a_{ij}
$\underline{S}$	Second Piola Kirchhoff Stress
W	Strain Energy Density Function
$\underline{L}^G$	Green-Lagrange Strain Tensor
I_i	Invariant of Strain Tensor
ϵ_{ij}	Green-Lagrange Strains
α	Cauchy Stress Tensor
κ	Bulk Modulus
ν	Poisson's Ratio

LIST OF ABBREVIATIONS

GT	Graston Technique
MT	Manual Therapy
LFMM	Linked fiber-matrix mesh
ECM	Extracellular Matrix
EDL	Extensor Digitorum Longus

1. INTRODUCTION

1.1 Skeletal Muscle

Skeletal muscle functions to generate force or to produce movement. Skeletal muscle is made up of individual muscle fibers that are the "building blocks" of the muscular system. These individual muscle fibers consist of myofibrils, which are divisible into individual filaments. The origin of a muscle is the end of the muscle that is attached closest to the trunk or to the more stationary bone. The insertion of the muscle is the more distal or mobile attachment. When the bones attached to a muscle are connected bones are brought closer together when the muscle contracts, the muscle is called a flexor. If the bones move away from each other when the muscle contracts, the muscle is then called an extensor.

The whole muscle is surrounded by fascia, which is a tough connective tissue which spreads throughout the body in a three-dimensional web. Generally the fascial system provides support, stability, and cushioning. It is also a system of locomotion and dynamic flexibility forming muscle. Tightening of the fascial system is a histological, physiological and biomechanical protective mechanism that is a response to trauma. The fascia looses its pliability, becomes restricted, and is a source of tension to the rest of the body. The ground substance solidifies, the collagen becomes dense and fibrous, and the elastin looses its resiliency. Over time this can lead to poor muscular biomechanics, altered structural alignment, and decreased strength, endurance and motor coordination. Subsequently, the patient is in pain and functional capacity is lost [6].

A further connective tissue known as epimysium covers the entire surface of the muscle belly and separates it from other muscles. It contains tightly woven bundles of collagen fibers that have a wavy appearance and are connected to the perimysium. The perimysium also tough and relatively thick: it divides the muscle into bundles,

or fascicles of fibers, and it also provides the pathway for the major blood vessels and nerves to run through the muscle belly. The endomysium envelops each muscle fiber and is composed of a dense feltwork of collagen fibrils, some of which are continuous with the fine fibrillar mesh of the perimysium (Fig 1.1).

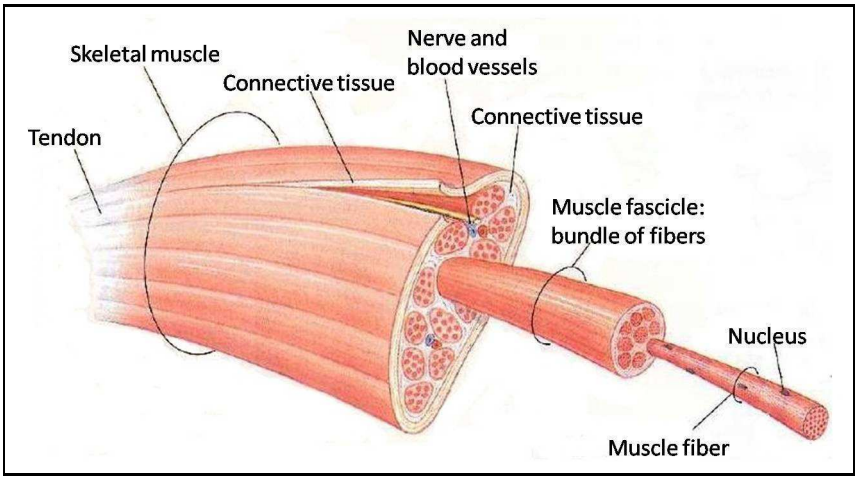

Figure 1.1 Schematic diagram of the organization of the skeletal muscle.

1.2 Structure of Muscle Fibers

The individual fibers of the skeletal muscle are bounded with connective tissue and arranged with their long axes in parallel (Fig 1.1). Collagen elastic fibers, nerves, and blood vessels are found between the bundles of muscle fibers and with the tendons holding the muscle to underlying bones. The cell membrane of a muscle fiber is called the sarcolemma.

Each muscle fiber contains a thousand or more myofibrils that occupy most of the intracellular volume, leaving little space for cytosol and organnales (Fig 1.2). Each myofibril is composed of several types of proteins: the contractile proteins myosin and actin, the regulatory proteins tropomyosin and troponin, and the giant accessory proteins titin and nebulin.

Myosin is the protein that makes up the thick filaments of the myofibril. Each myosin molecule is composed of two heavy protein chains that intertwine to form a

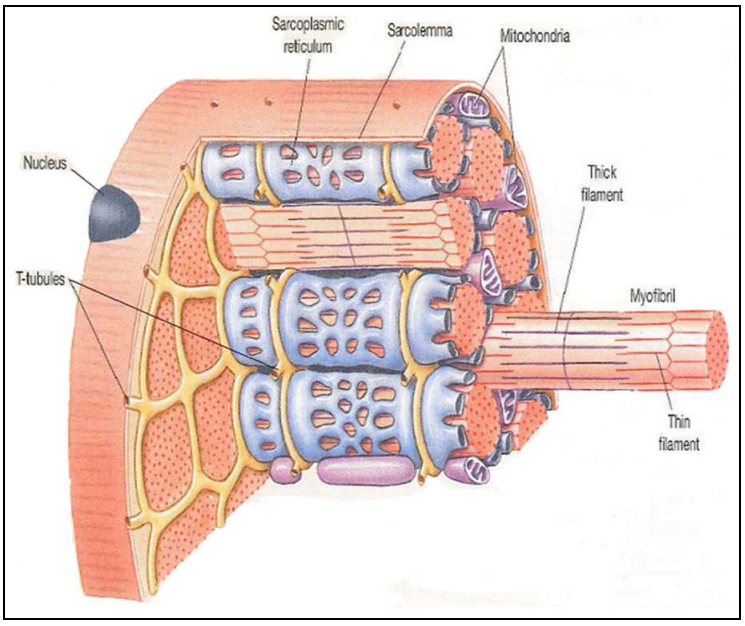

Figure 1.2 Schematic diagram of the organization of the muscle fiber.

long coiled tail and a pair of tad-polelike heads. Two lightweight protein chains are associated with the heavy chain of each head. The thick filament is arranged so that the myosin heads are clustered at the ends, and the central region of the filament is a bundle of the myosin tails. The rodlike portion of the thick filament is stiff, but the protruding myosin heads have an elastic hinge region allows the heads to swivel around their point of attachment.

Actin, is the protein that makes up the thin filaments of the muscle fiber. In skeletal muscle, two F-actin polymers twist together like a double strand of beads, creating the thin filaments of the myofibril.

Most of the time, the parallel thick and thin filaments of the myofibril are connected by cross-bridges that span the space between the filaments. The cross-bridges are the myosin heads that loosely bind to the actin filaments. Under a light microscope, the arrangement of the thick and thin filaments in a myofibril creates a repeating pattern of light and dark bands(Figure 1.3)[1]. One repeating pattern forms a sarcomere which has the following elements:

Z disk: These zigzag structures are made up of proteins that serve as the attachment sites for the thin filaments. One sarcomere is composed of the two Z disks and the filaments found between them.

I band: These are the lightest color bands of the sarcomere and represent a region occupied only by thin filaments.

A band: This is the darkest of the bands in a sarcomere and encompasses the entire length of a thick filament. At the outer edges of the A band, the thick and thin filaments overlap. The center of the A band is occupied by thick filaments only.

H zone: This central region of the A band is lighter than than the outer edges of A band because the H zone is occupied thick filaments only.

M line: This band represents the attachment site for the thick filaments equivalent to the Z disk for the thin filaments.

The proper alignment of filaments within a sarcomere is ensured by two types of proteins, titin and nebulin. Titin is huge elastic molecule and stretches from one Z disk to the next M line. It has two functions: (1)it stabilizes the position of the contractile filaments, and (2) its elasticity returns stretched muscles to their resting length.

1.3 Manual Therapy Treatment

Manual therapy encompasses a broad range of techniques that are used to treat patients with musculoskeletal disorders (i.e. cerebral palsy, tendinopathy, lower back pain, osteoarthritis, etc.). In these diseases, abnormal shortness of the muscle and tendon lead to muscle dysfunction, joint immobility, and pain [7, 8].

Manual therapy techniques (i.e. friction, myofascial release, traction, articulation/ thrust effleurage, petrissage/ kneading, stroking and long-axis tractioning, iso-

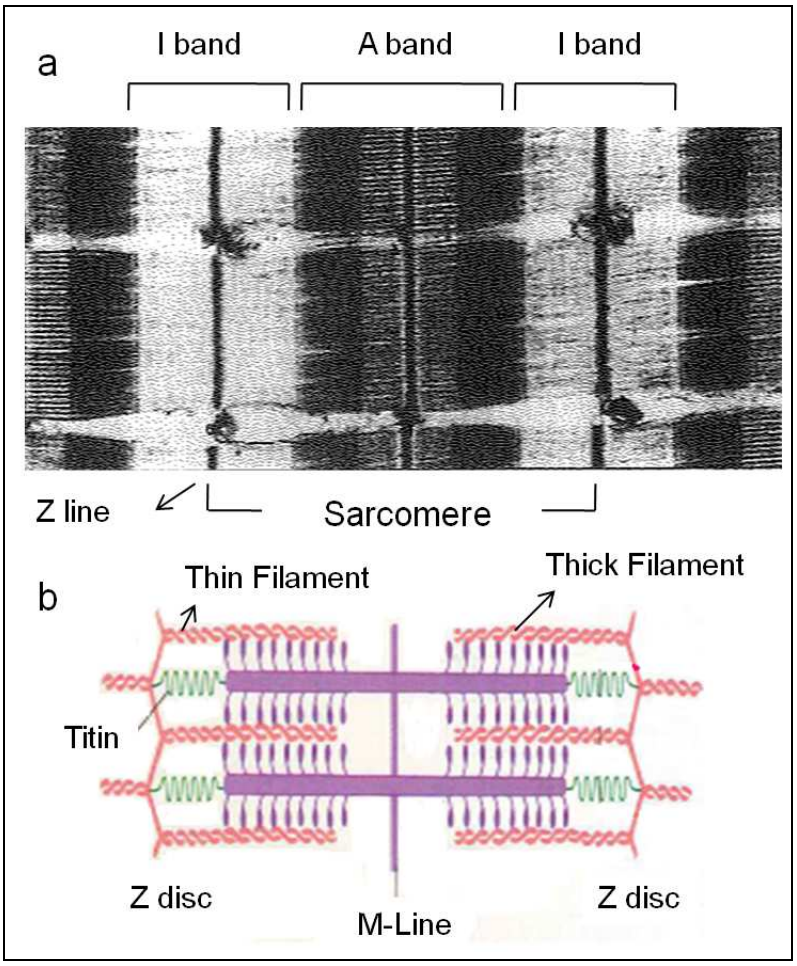

Figure 1.3 (A)Longitudinal electron micrograph of several myofibrils, showing the characteristic striation, (B) Schematic representation of myofilaments.[1, 2]

metric agonist contraction, includes manipulation and stretching techniques, graded manual therapeutic techniques)[7, 9, 3] . Manual therapy is particularly aimed at the improvement of elasticity of the joint capsule and the surrounding muscles . One of the aims of manual therapy is to permanently elongate the soft tissues that are restraining joint mobility through the application of specific external forces. It is important to note that a low level of damage must occur in order to produce permanent elongation. Therefore, manual therapists aim for microfailure of tissues to achieve this elongation. *Microfailure* represents the breakage of individual collagen fibers and fiber bundles that are placed under tension during progressive deformation. The remaining intact fibers and bundles that may have not been directly aligned with the force or those that had more intrinsic length absorb a greater portion of the load. The result is progressive, permanent (plastic) elongation of structures. If the forces are released, the broken fibers

will not contribute to the recoil of the tissue. A new length of the tissue is established that reflects the balance between the elastic recoil of the remaining intact collagen and the resistance of the intrinsic tissue water and glycosaminoglycans to compression. The collagen breakage will be followed by a classical cycle of inflammation, repair, and remodeling that should be therapeutically managed in order to maintain the desired tissue elongation [7, 10].

During therapy, direction of loading, period of applied load, frequency and duration of therapy session are important aspects of treatment and they must be held scientifically. Manual therapy is provided by physical therapists (or medical doctors) with a special training in manual therapy.

1.3.1 Instrument Assisted Manual Therapy

Manual therapy is also applied with special instruments and Graston technique(GT) is one of the widely used treatment. Graston technique is a patented form of treatment using stainless steel instruments designed with a unique curvilinear treatment edge, contoured to fit various shapes of the body.While GT is used to mechanically mobilize scar tissue, increasing its pliability and loosening it from surrounding healthy tissue, it is hypothesized that for degenerated connective tissue GT re-initiates the inflammatory process by introducing a controlled amount of microtrauma to the affected area. A healing cascade is created by enhancing the proliferative invasion of blood, nutrients, and fibroblasts to the region resulting in collagen deposition and eventual maturation. Graston technique instruments and some of its applications are shown in Figure 1.4.

1.4 Goal of the Study

At present, there is a lack of research studies in the field of manual therapy; therefore the magnitude of the applied mechanical forces, direction of the loading, and

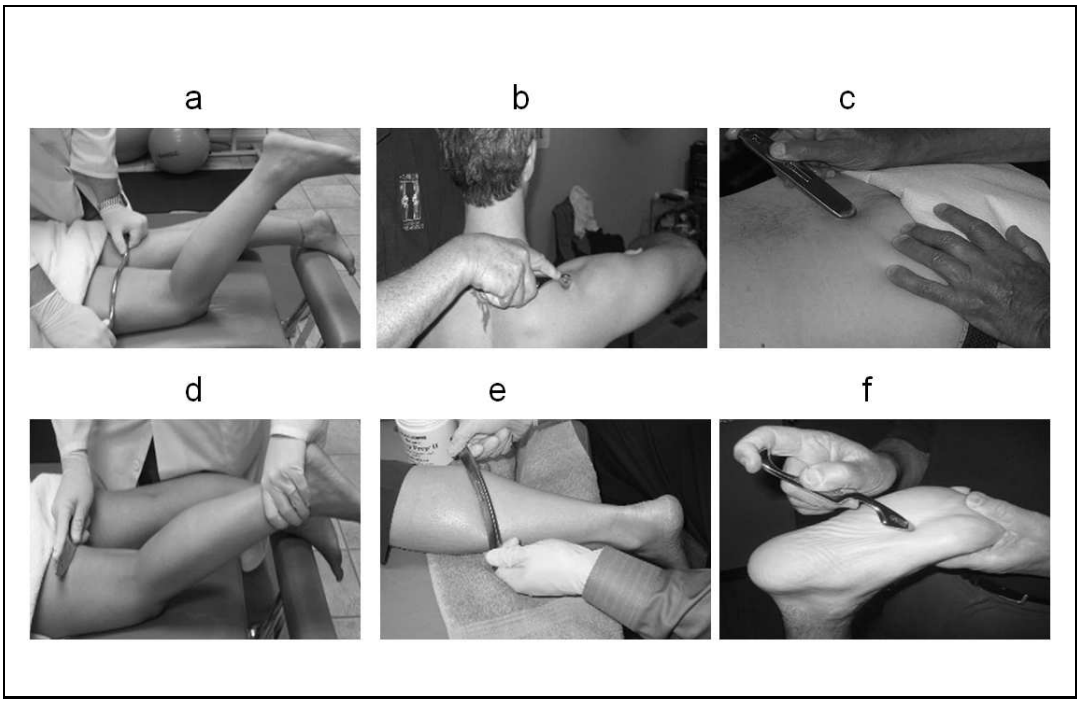

Figure 1.4 Six Graston Technique instruments and their applications. (A) Treating Hamstrings during active motion using GT 1 [3], (B) GT 2 for musculotendinous portion of supraspinatus [3], (C) Use of GT 3 for local release of tissue in the lumbosacral area [4], (D) Treating Hamstrings during motion using GT 4 [3], (E) Treating gastrocnemius/soleus using GT 5 [3] (F) GT 6 treating distal plantar fascia [3]

duration of the loading are clearly not known. These mechanical properties of soft tissues that are established in vivo should be scientifically determined during manual therapy treatment [11, 12].

A second benefit of the identification of MT mechanisms is the potential for increased acceptance of these techniques by healthcare providers. Despite the literature supporting the effectiveness of MT in specific musculoskeletal conditions, healthcare practitioners at times provide or refer for MT at a lower rate than expected rate. Such lack of an identifiable mechanism of action for MT may limit the acceptability of these techniques as they may be viewed as less scientific. Knowledge of mechanisms may promote more optimal use of MT by healthcare providers as well. [13]

In the present study, a quantitative appraoch to loading situations, effects of which may be representative of the effects of manual therapy on muscular mechanics was aimed to have a better understanding of the procedure.

2. METHODS

2.1 Description of the "Linked Fiber-Matrix Mesh Model"

In this study, the linked fiber-matrix mesh(LFMM) model of Yucesoy et al.(2002) will be used. In this model, two self-programmed 3D elements were introduced as user-defined elements into the finite element program ANSYS 9.0. One of the elements represents the extracellular matrix, which includes the basal lamina and connective tissue components such as endomysium and perimysium (*extracellular matrix element*). The other element represents the muscle fibers (*myofiber element*). In the linked fiber-matrix mesh model(LFMM model), skeletal muscle is considered explicitly as two separate domains: (1) the intracellular domain and (2) Extracellular matrix (ECM) domain. The transsarcolemmal attachments are considered as elastic links between the two domains [5].

Within the biological context, the combined *muscle element* represents a segment of a bundle of muscle fibers with identical material properties, its connective tissues and the links between them. This is realized as a linked system of ECM and myofiber elements. A schematic 2D representation of an arrangement of these muscle elements is shown in Figure 2.1.

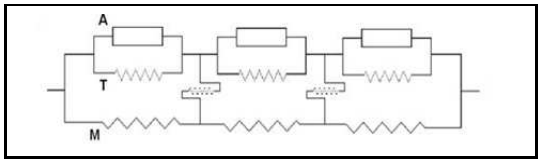

Figure 2.1 Two-dimensional-schematic representation of an arrangement of muscle elements. The intracellular domain, which is composed of the active contractile elements (A) and intracellular passive cytoskeleton (T), is linked to the extracellular matrix domain (M) elastically [5]

In the LFMM model, the ECM domain is represented by a mesh of ECM elements (*matrix mesh*). In the same space, a separate mesh of myofiber elements is built to represent the intracellular domain (*fiber mesh*). The two meshes are rigidly connected to single layers of elements modeling proximal and distal aponeuroses at the

myotendinous connection sites and are linked elastically at the intermediate nodes. For these links (the model includes a total of 28 of them: 14 in each of the upper and lower model surfaces) the standard element, COMBIN39 is used from the element library of ANSYS 9.0. This is a 2-node spring element, which is set to be uniaxial and have linear high stiffness characteristics representing non-pathological connections between the muscle fibers and the extracellular matrix. Note that at the initial muscle length and in passive condition, these links have a length equaling zero.A typical geometry for the model is shown in Figure 2.2.

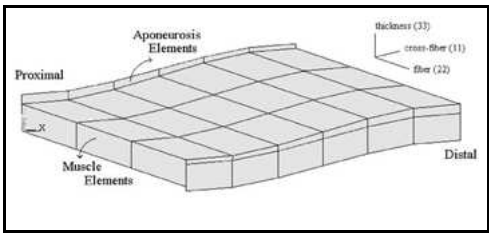

Figure 2.2 The geometry of the muscle model is currently defined by the contour of a longitudinal slice of the isolated rat medial gastrocnemius muscle belly. The model is composed of three in series and six in parallel muscle elements. A 3D local coordinate system representing the fiber, crossfiber (direction perpendicular to the fiber direction) and thickness directions used for the analysis and presentation of the results is shown. Proximal and distal ends of the model were restrained in all directions. The nodes at the lower surface of the model were constrained to move in the thickness direction [5].

Extracellular matrix and myofiber elements have eight nodes; linear interpolation functions and a large deformation analysis formulation are applied. A 3D local coordinate system representing the fiber, cross-fiber (normal to the fiber direction), and thickness directions is used. The stress formulation, $\underline{S}$ based on Second Piola-Kirchoff definition constitutes the derivative of the strain energy density function, W with respect to the Green-Lagrange strain tensor, $\underline{L}^G$:

$$\underline{S} = \frac{dW}{d\underline{L}^G} \tag{2.1}$$

2.1.1 Extramuscular Matrix Element

The strain energy density function mechanically characterizing the extracellular matrix includes two parts:

$$W = W_1 + W_2 \tag{2.2}$$

The first part represents the non-linear and anisotropic material properties [14]:

$$W_1 = k.(e^{a_{ij}.z_{ij}} - a_{ij}.\epsilon_{ij}) \; for \; \epsilon_{ij} > 0 \; or, \tag{2.3}$$

$$W_1 = -W_{ij}(|\epsilon_{ij}|) \; for \; \epsilon_{ij} < 0 \; and \; i \neq j \tag{2.4}$$

where ϵ_{ij} are the Green-Lagrange strains in the local coordinates. The indices $i = 1, ..., 3$ and $j = 1, ..., 3$ represent the local cross-fiber, fiber and thickness directions respectively. a_{ij} and k are constants (Table 2.1). Note that, initial passive stiffness (k) and passive fiber direction stiffness (a_{22}) values were estimated by fitting the experimental data by Meijer et al. Based on the experimental data on dog diaphragm [15], passive cross-fiber stiffness ($a_{11} = a_{33}$) was taken to be higher than fiber direction stiffness. Identical values are used for fiber and fiber-cross fiber shear stiffness ($a_{12} = a_{23} = a_{31}$). However, in contrast to the non-symmetric stress-strain relationships defined for fiber and cross-fiber directions, a symmetric stress-strain relationship is used for shearing (Figure 2.3).

The second part of Eqn 2.2 includes a penalty function to account for the con-

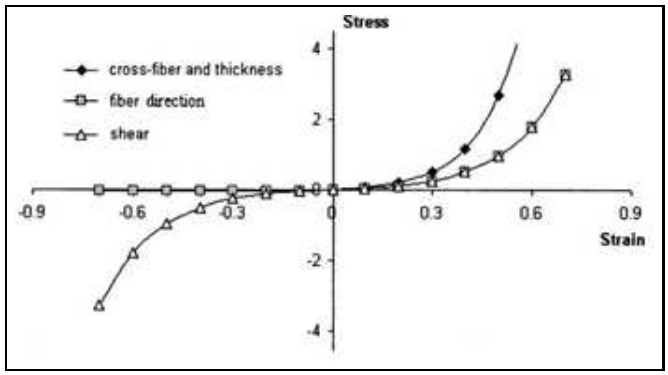

Figure 2.3 The stress-strain relation representing the mechanical behavior of passive non-linear and anisotropic material properties of the extracellular matrix element in the local coordinates[5].

stancy of muscle volume. The intracellular fluid and solid elastic structures are considered as separate constituents of muscle tissue with different responses to deformation: The intracellular fluid is assumed to have the ability to migrate freely within the cell, whereas, the solid elastic structures housing muscle fibers (e.g. basal lamina and endomysium) are restricted in moving as they are being constrained by neighboring cells. Therefore, a penalty function consisting of two parts was used:

$$W_2 = S_s.(I_3 - 1)^2 + S_f.(I_{avg}^3 - 1) \tag{2.5}$$

where I_3 is the third invariant (determinant) of the Right Cauchy-Green strain tensor providing a ratio of the deformed local volume over the undeformed local volume for each Gaussian point.

If all I_3's are kept as unity, the element is considered as solid and the local volumes are conserved. If the weighted mean of all I_3's per element, (I_{avg}^3) is kept as unity, the element is considered as a fluid. The penalty parameters S_s (for the solid volume) and S_f (for the fluid volume), allow determining the penalty given for each part. Note that if both I_3's and (I_{avg}^3)'s are unity the volume is constant. The parameters S_s and S_f (Table 2.1) chosen after performing specific tests on the extracellular matrix element allow a good representation of constancy of muscle volume with opti-

mal numerical efforts: for even very large deformations (e.g. length changes greater than 40%) the maximal deviation from undeformed volume remains below 5% .

2.1.2 Myofiber Element

Maximally activated muscle is studied. Sarcomeres within the muscle fibers are assumed to have identical material properties. The force-velocity characteristics are not considered due to the isometric nature of the present work. The total stress for the intracellular domain (σ_{22_f}) is a Cauchy stress acting in the local fiber direction exclusively and is the sum of the active stress of the contractile elements ($\sigma_{22_{contr}}$) and the stress due to intracellular passive tension ($\sigma_{22_{icp}}$).

To define the active length-force characteristics, an exponential function (Figure 2.3) was fit to the experimental data of isolated small rat gastrocnemius medialis fiber bundles [16]. This function is scaled such that at optimum length, the fiber direction strain (ϵ_{22}) is zero and the maximal stress value is unity.

$$\sigma_{22_{contr}}(\epsilon_{22}) = b_3 e^{b_2 \epsilon_{22}^3} \; for \; \epsilon_{ij} > 0 \; or, \tag{2.6}$$

$$\sigma_{22_{contr}}(\epsilon_{22}) = b_3 e^{b_1 \epsilon_{22}^4} \; for \; \epsilon_{ij} < 0 \tag{2.7}$$

where b_1, b_2 and b_3 are constants

The source of intracellular passive tension is the intra-sarcomeric cytoskeleton [17], which is composed of several proteins. In this work titin is considered to play the dominant role. Experimental tension-sarcomere length data [17] for a single rabbit skeletal muscle fiber was fitted using a parabolic function and scaled to make it compatible to the stress-strain characteristics of the contractile part(Figure 2.4).

$$\sigma_{22_{contr}}(\epsilon_{22}) = t_1\epsilon_{22}^2 + t_2\epsilon_{22} + t_3 \; for \; \epsilon_{22} > 0 \; and \tag{2.8}$$

$$\sigma_{22_{contr}}(\epsilon_{22}) = 0 \; for \; \epsilon_{22} < 0 \tag{2.9}$$

where t_1, t_2, and t_3 are constants.

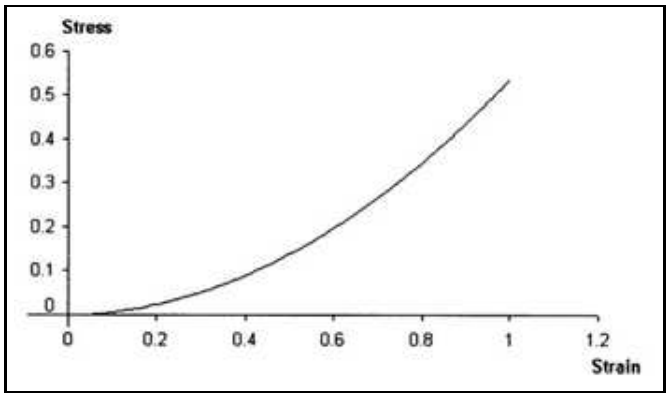

Figure 2.4 Mechanical properties representing the titin filaments which is dominating the passive resistance in the myofiber element in the local fiber direction. The stresses are normalized and dimensionless[5].

2.1.3 Aponeurosis Element

In order to represent the aponeuroses, a standard 3D, 8-node element HYPER58, from the element library of ANSYS 9.0 is used. This element has a hyperelastic mechanical formulation for which the strain energy density function is defined using the two parameter Mooney-Rivlin material law:

$$W = a_{10}(\overline{I}_1 - 3) + a_{01}(\overline{I}_2 - 3) + \frac{K}{2}(\overline{I}_3 - 1)^2 \tag{2.10}$$

where, $\overline{I}_i$ are reduced invariants of right-Cauchy strain tensor for $i = 1, ..., 3$, a_{10}

and a_{01} are Mooney-Rivlin material constants, $K = 2(a_{10} + a_{01})/(1 - 2\nu)$ is the bulk modulus and ν is the Poisson's ratio. The parameters used (Table 2.1) ensure sufficient stiffness for the aponeuroses for a representative role in force transmission and providing muscular integrity as in real muscle.

It is assumed that, at the initial muscle length in the passive state, the sarcomeres arranged in series within muscle fibers have identical lengths. Local strain, as a measure of change of length, reflects the lengthening (positive strain) or shortening (negative strain) of sarcomeres. Note that zero strain in the model represents the undeformed state of sarcomeres (i.e., sarcomere length $\cong 2.5$ μm) in the passive condition at initial muscle length (28.7 mm). Fiber direction strain within the fiber mesh of the LFMM model was used to assess the non-uniformity of lengths of sarcomeres arranged in-series within muscle fibers.

2.2 EDL muscle models with extramuscular connections

EDL muscle of the rat was modeled. This muscle has a relatively simple geometry: it is a unipennate muscle with rather small pennation angles and minimal variation of the fiber direction within the muscle belly. The geometry of the model (Figure 2.2) is defined as the contour of a longitudinal slice at the middle of the isolated rat EDL muscle belly. Three muscle elements in series and six in parallel fill this slice. All aponeurosis elements have identical mechanical properties but using a variable thickness in the fiber-cross fiber plane, the increasing cross-sectional area of the aponeurosis toward the tendon[18] is accounted for.

An extramuscular connective tissue connects EDL all along the muscle to the tibia, part of interosseal membrane and anterior intermuscular septum. In an experimental study, the locations of the extramuscular connections to EDL muscle were determined to be predominantly at one-third of the fascicle length from the most proximal end of each muscle fascicle [19]. In that study, it was also shown that the neurovascular tract (i.e. extramuscular connective tissue structure embedding and re-

inforcing nerves and blood vessels) supplying the EDL muscle proximally are much stiffer than the distal of the connective tissue structure [20].

In order to model the muscles' extramuscular connections and to account for their continuity with the muscular extracellular matrix, a set of nodes of the matrix mesh were linked using spring elements (COMBIN39, from the element library of ANSYS 9.0) to a set of fixed points. Our modeling considerations were: (1) the set of fixed points comprising "mechanical ground" represent bone, which is assumed to be rigid. (2) the spring elements modeling the muscles' extramuscular connections were set to be uniaxial and have linear length-force characteristics. (3) Initially (i.e. muscle length = 28.7 mm, and before changing any of the tendon positions), the fixed points and the corresponding nodes of the model were at identical locations (i.e., the spring elements modeling the muscles' extramuscular connections were at a length of zero). (4) The higher stiffness of the connective tissues constituting the neurovascular tract near the EDL muscle is taken into account by making the three most proximal links to the muscle stiffer than distal ones. Stiffness values determined previously were used (i.e. k = 0.286 unit force/mm for stiffer part and, k = 0.067 unit force/mm for the more distal links)[19].

2.3 Solution Procedure

The analysis type used in ANSYS was static and large strain effects were included. During the entire solution procedure, the models studied were stable and no mesh refinement was performed. A force based convergence criterion was used with a tolerance of 0.5

Initially, at the passive state, the activation coefficient b_3 (eqn. 2.6) equaled 0. Maximal activation of the muscles modeled was achieved by increasing incrementally up to 1, using fixed increments. Subsequent to activation, in order relatively position the muscle, the proximal and the distal end of the modeled muscles were displaced proximally by 2.5 mm and distally by 2.5 mm which positions were then kept constant

during entire modeling.

2.4 Assessment of the Effects of Manual Therapy

In order to analyze the effects of manual therapies, disturbance was applied to selected locations of the model. EDL muscle with extramuscular links was modeled in several conditions including loading on single location on proximal aponeurosis and multiple loading (i.e. two locations simultaneously) on proximal aponeurosis at i) location P exclusively (Case P), ii) location I exclusively (Case I), iii) location D exclusively (Case D), iv) locations P and I (Case P-I), and v) locations I and D (Case I-D). 'No manual therapy case' refers to the muscle in its initial length (i.e., 28.7 mm) that is located relatively to its neighboring muscles. For the case that there is no study available to quantify the magnitudes of forces applied during manual therapy, such disturbance will be applied in terms of displacements [11]. In order to model compression and tensioning techniques, displacements were applied towards -y direction and + y direction in the global coordinates of the model, respectively. The values of different modeled conditions were attributed for convergence criterion of the solution. Beyond a certain value of therapeutic loading the solution did not converge; as a result, these values were obtained from the modeled therapeutic loading for every loading condition.

1.Single Therapeutic Loading:

1.1 Single Location Loading in Compression on Passive Muscle Model

1.2 Single Location Loading in Tension on Passive Muscle Model

1.3 Single Location Loading in Compression on Activated Muscle Model

1.4 Single Location Loading in Tension on Activated Muscle Model

2. Multiple Therapeutic Loading:

2.1 Multiple Location Loading in Compression on Passive Muscle Model

2.2 Multiple Location Loading in Tension on Passive Muscle Model

2.3 Multiple Location Loading in Compression on Activated Muscle Model

2.4 Multiple Location Loading in Tension on Activated Muscle Model

In our model, stretching effect was realized by positioning the muscle relative to its nonmuscular neighboring structures and compression or tensioning load was realized by applying a downward or an upward displacement, respectively. The locations of applied displacements (e.g. Location P, Location I, and Location D) are shown in Figure 2.5. The strain distributions in the local fiber and cross-fiber directions calculated for active and passive muscle models after single and multiple loading were compared to no manual therapy case 'Case no MT' (a case where the muscle model was not loaded as a representation of manual therapeutic loading) and Case P, respectively.

In order to quantitatively assess the local effect of manual therapy, percentage changes of nodal strains were compared to the reference case (i.e. Case no MT). These percentage changes of nodal strains were calculated for the nodes (node number 22-26 on the first row and node number 32-36 on the second row (see Figure 2.5) that are near the locations of applied single or multiple displacements.

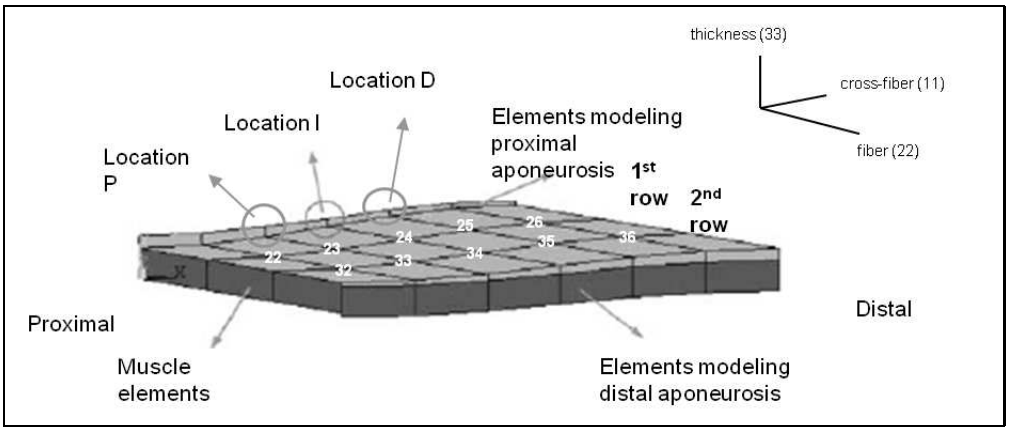

Figure 2.5 The geometry of the muscle model is currently defined by the contour of a longitudinal slice of the isolated rat medial gastrocnemius muscle belly. The model is composed of three in series and six in parallel muscle elements. A 3D local coordinate system representing the fiber, crossfiber (direction perpendicular to the fiber direction) and thickness directions used for the analysis and presentation of the results is shown. Proximal and distal ends of the model were restrained in all directions. The nodes at the lower surface of the model were constrained to move in the thickness direction. The Figure is modified from [5].

Table 2.1
Values and definitions of the model constants

	Value	Unit	Definitions
k	0.05	N/mm2	Initial passive stiffness (Eq 2.4)
a_{11}	8.0	-	Passive cross-fiber direction stiffness ($a_{11} = a_{33}$
a_{22}	6.0	-	Passive fiber direction stiffness (Eq 2.4)
a_{12}	6.0	-	Passive fiber-cross-fiber shear stiffness, ($a_{12} = a_{23} = a_{31}(Eq2.4)$
S_s	10.0	N/mm2	Weight factor in the penalty function for the solid volume (Eq. 2.5)
S_f	10.0	N/mm2	Weight factor in the penalty function for the fluid volume (Eq. 2.5)
b_1	30.0	-	Coefficient for the stress-strain relation of the contractile elements (Eq 2.6)
b_2	-6.0	-	Coefficient for the stress-strain relation of the contractile elements (Eq 2.6)
b_3	1	-	Coefficient for the stress-strain relation of the contractile elements (Eq 2.6)
t_1	0.522	-	Coefficient for the stress-strain relation of the intracellular passive elements (Eq 2.7)
t_2	0.019	-	Coefficient for the stress-strain relation of the intracellular passive elements (Eq 2.7)
t_3	-0.002	-	Coefficient for the stress-strain relation of the intracellular passive elements (Eq 2.7)
a_{10}	7.9	N/mm2	Mooney-Rivlin material constant for aponeurosis elements (Eq. 2.8)
a_{01}	7.9	N/mm2	Mooney-Rivlin material constant for aponeurosis elements (Eq. 2.8)
ν	0.3	-	Poisson's ratio for aponeurosis elements (Eq. 2.8)

3. RESULTS

3.1 Effects of Location and Direction of Single Location Loading

3.1.1 Loading in Compression on Passive Muscle Model

A downward displacement of 0.65 mm was applied to account for a compressive manual therapy technique. The passive muscle model was positioned relative to its nonmuscular neighboring structures. Note that '-' and '+' signs in inserts above the bars indicate relative shortening and lengthening, respectively. For example, for Figure 3.2a the strain values of node number 22 changed from a negative value to another negative value.

1. The area of positive strains in fiber direction and the area of cross-fiber direction strain distributions were increased for the Case P compared to Case no MT (Figure 3.1a and 3.1b). Strain is defined as the ratio of the change in length to the original length, and a positive strain indicates the lengthening of the sarcomeres with respect to its undeformed state (i.e., sarcomere length= 2.5mm).

2. In Figure 3.2a and 3.2b, it can be seen that the highest increases (equaling 78% for first row and 61% for second row in percentage change of fiber direction strains are at the most proximal nodes of the rows.

3. Figures 3.2c and 3.2d show that the highest increases (equaling 233 % for first row and 292 % for second row in percentage change of cross-fiber direction strains are at the most distal nodes of the rows.

The values of node 25 and node 26 in Figure 3.2a were not used because the strain took a more negative value, and the value of node 32 in Figure 3.2d was not used

because the strain changed from a positive value to a negative value due to therapeutic loading.

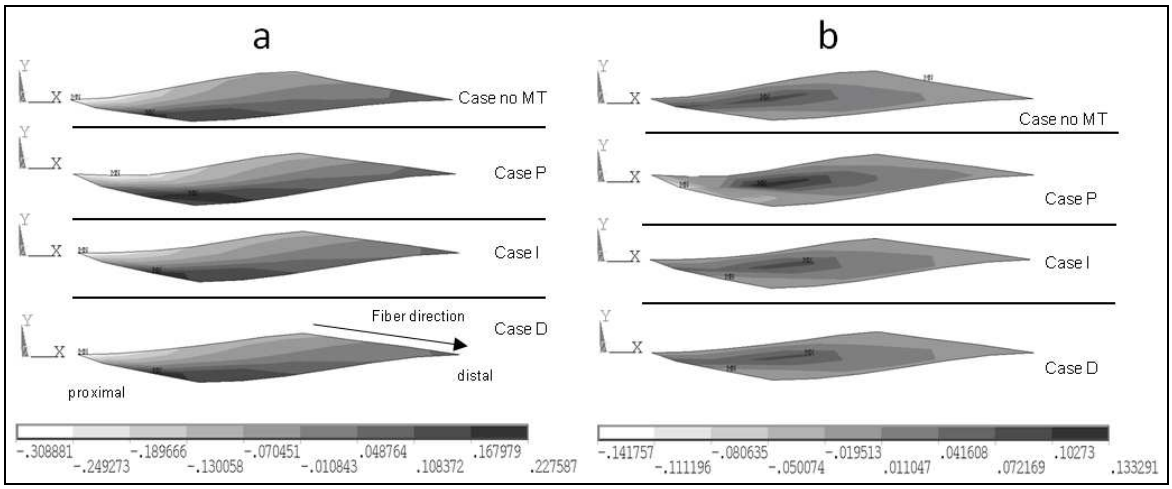

Figure 3.1 (A)Fiber direction strains within modeled passive muscle. The muscle is in its initial length and positioned relative to its nonmuscular neighboring structures. Compressive load is applied towards -y direction, (B)Cross-fiber direction strains within modeled passive muscle. The muscle is in its initial length and positioned relative to its nonmuscular neighboring structures. Compressive load is applied towards -y direction.

3.1.2 Loading in Compression on Active Muscle Model

A downward displacement of 0.3 mm was applied to account for a compressive manual therapy technique. The active muscle model was positioned relative to its nonmuscular neighboring structures.

1. The area of positive strains in fiber direction and also in cross-fiber direction strain distributions was increased for the case P compared to Case no MT (Figure 3.3).

2. In Figure 3.4a and 3.4b, it can be seen that the highest increases (equaling 25% for first row and 2234 % for seccond row in percentage change of fiber direction strains are at the most proximal nodes of the rows.

3. Figures 3.4c and 3.4d show that the highest increases (equaling 35 % for first row and 117 % for second row in percentage change of cross-fiber direction strains

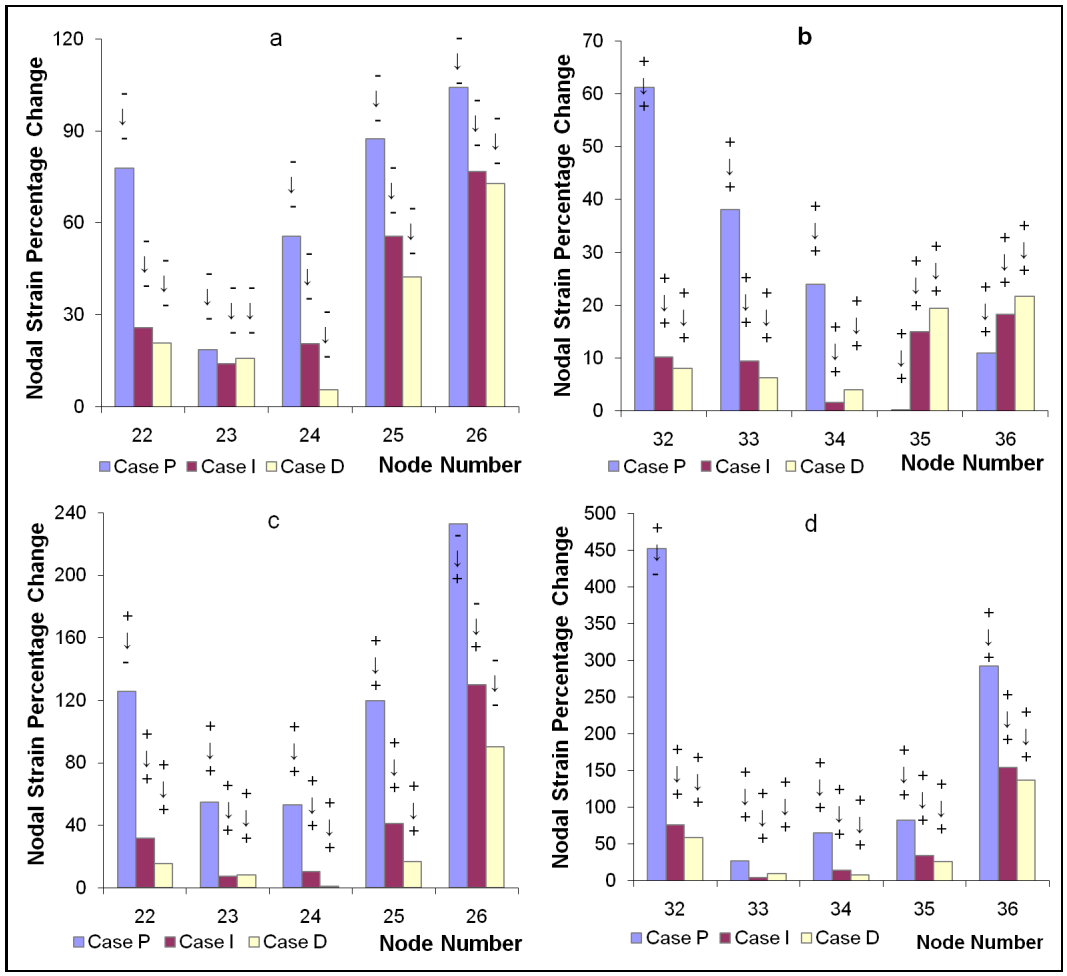

Figure 3.2 (A)Comparison of percentage changes of fiber direction nodal strain values compared to Case no MT for first row. (B)Comparison of percentage changes of fiber direction nodal strain values compared to Case no MT for second row, (C)Comparison of percentage changes of cross-fiber direction nodal strain values compared to Case no MT for first row, (D)Comparison of percentage changes of cross-fiber direction nodal strain values compared to Case no MT for second row.

are at the proximal part of the muscle for first row and at the distal part of the muscle for second row.

The value of node 22 in Figure 3.4c was not used because the strain showed a decrease in value even if it was positive, and the value of node 36 in Figure 3.4d was used because the other strain values changed from a positive value to a negative value or from a positive value to a less positive value after treatment.

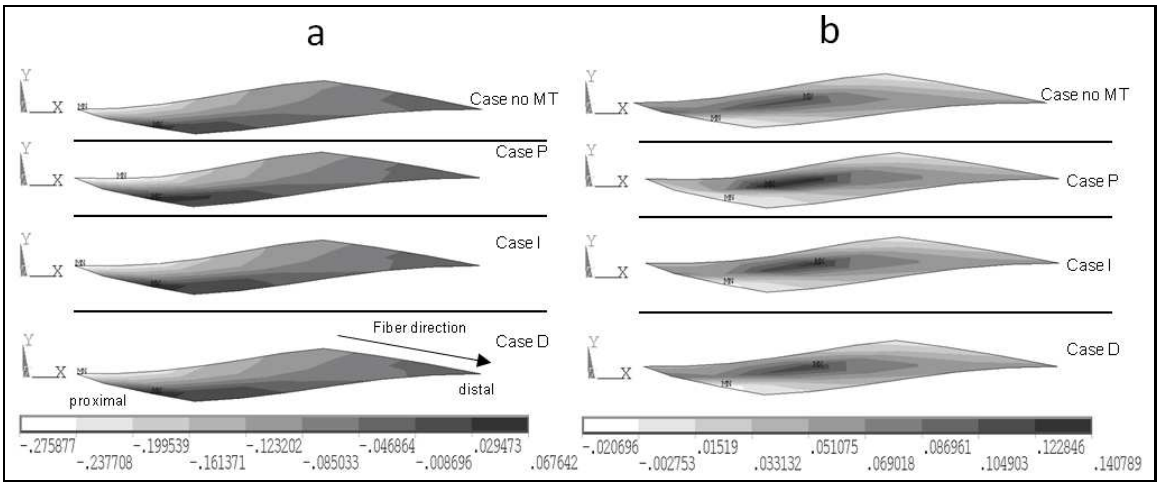

Figure 3.3 (A)(A)Fiber direction strains within modeled active muscle. The muscle is in its initial length and positioned relative to its nonmuscular neighboring structures. Compressive load is applied towards -y direction, (B)Cross-fiber direction strains within modeled active muscle. The muscle is in its initial length and positioned relative to its nonmuscular neighboring structures. Compressive load is applied towards -y direction.

3.1.3 Loading in Tension on Passive Muscle Model

An upward displacement of 0.925 mm was applied to account for a tensioning manual therapy technique. The passive muscle model was positioned relative to its nonmuscular neighboring structures.

1. The area of positive strains in fiber direction and the area of positive strains in cross-fiber direction strain distributions were increased for Case P compared to Case no MT (Figure 3.5).

2. In Figure 3.6a and 3.6b, it can be seen that the highest increases (equaling 129 % for first row and 60 % for second row) in percentage change of fiber direction strains are at the distal end of the muscle.

3. Figures 3.6c and 3.6d show that the highest increases (equaling 48 % for first row and 41 % for second row) in percentage change of fiber direction strains are at the most proximal nodes.

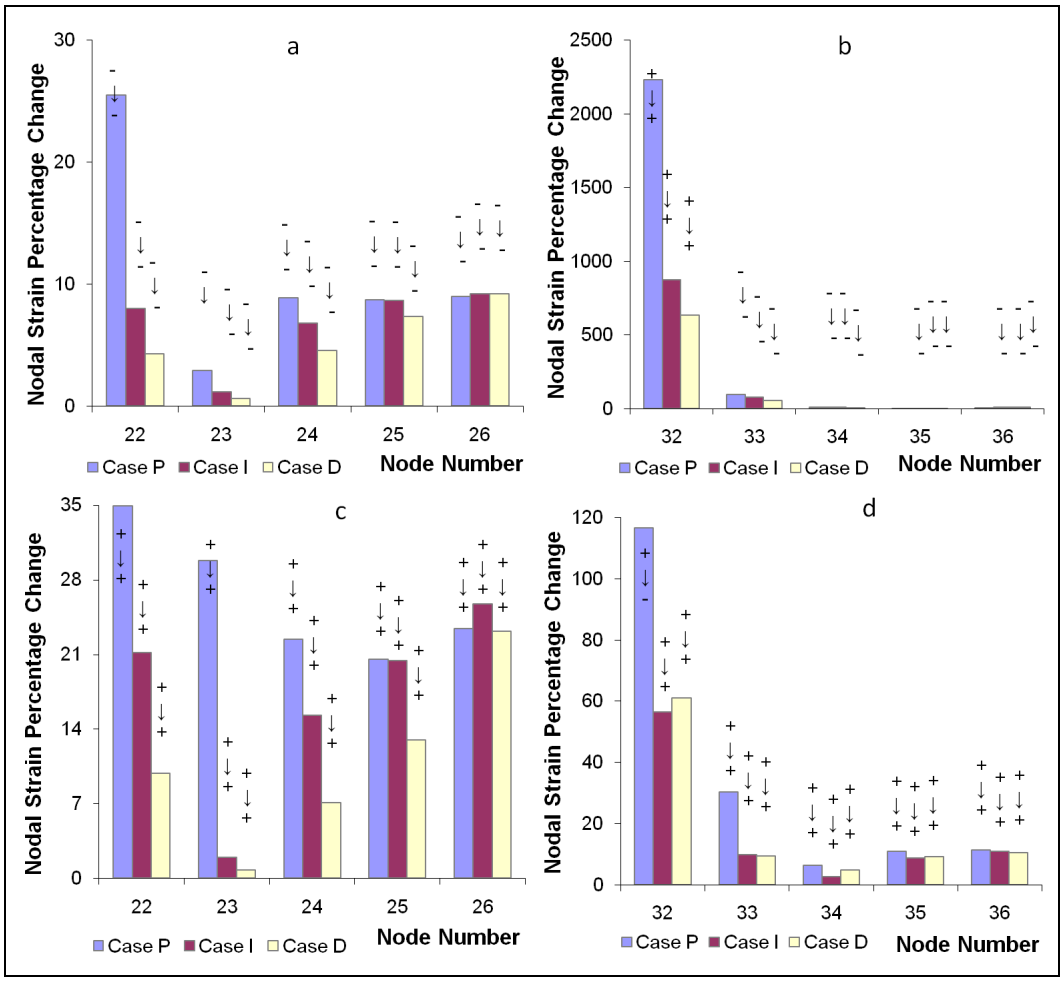

Figure 3.4 (A)Comparison of percentage changes of fiber direction nodal strain values compared to Case no MT for first row. (B)Comparison of percentage changes of fiber direction nodal strain values compared to Case no MT for second row, (C)Comparison of percentage changes of cross-fiber direction nodal strain values compared to Case no MT for first row, (D)Comparison of percentage changes of cross-fiber direction nodal strain values compared to Case no MT for second row.

The value of node 26 in Figure 3.6c was not used because it changed from a negative value to a more negative value. For Figure 3.6d, node 32 and 36 were not taken because the strains changed from a positive value to a negative value.

3.1.4 Loading in Tension on Active Muscle Model

An upward displacement of 1.0375 mm was applied to account for a tensioning manual therapy technique. The active muscle model was positioned relative to its nonmuscular neighboring structures.

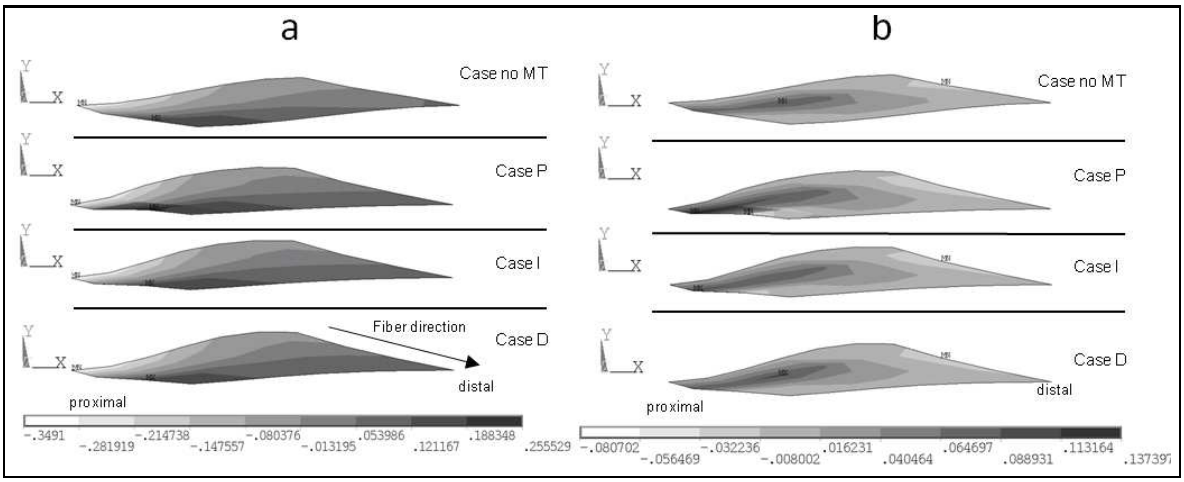

Figure 3.5 (A)Fiber direction strains within modeled passive muscle. The muscle is in its initial length and positioned relative to its nonmuscular neighboring structures. Tensioning load is applied towards +y direction. (B)Cross-fiber direction strains within modeled passive muscle. The muscle is in its initial length and positioned relative to its nonmuscular neighboring structures.

1. The areas of positive strains in fiber direction and cross-fiber direction strain distributions were decreased for all cases compared to no MT case (Figure 3.7).

2. In Figure 3.8a and 3.8b, it can be seen that the highest increases (equaling 27 % for first row and 59 % for second row) in percentage change of fiber direction strains are at the most proximal nodes of the rows.

3. Figures 3.8c and 3.8d show that the highest increases (equaling 20 % for first row and 85 % for second row) in percentage change of cross-fiber direction strains are at the most distal nodes of the rows.

In Figure 3.8b, the value of node 32 was not used because it changed from a positive value to a negative value, and node 33 was not used because it changed from a negative value to a more negative value. In Figure 3.8c, value of node 22 was used because the other values changed from a positive value to a less negative value.

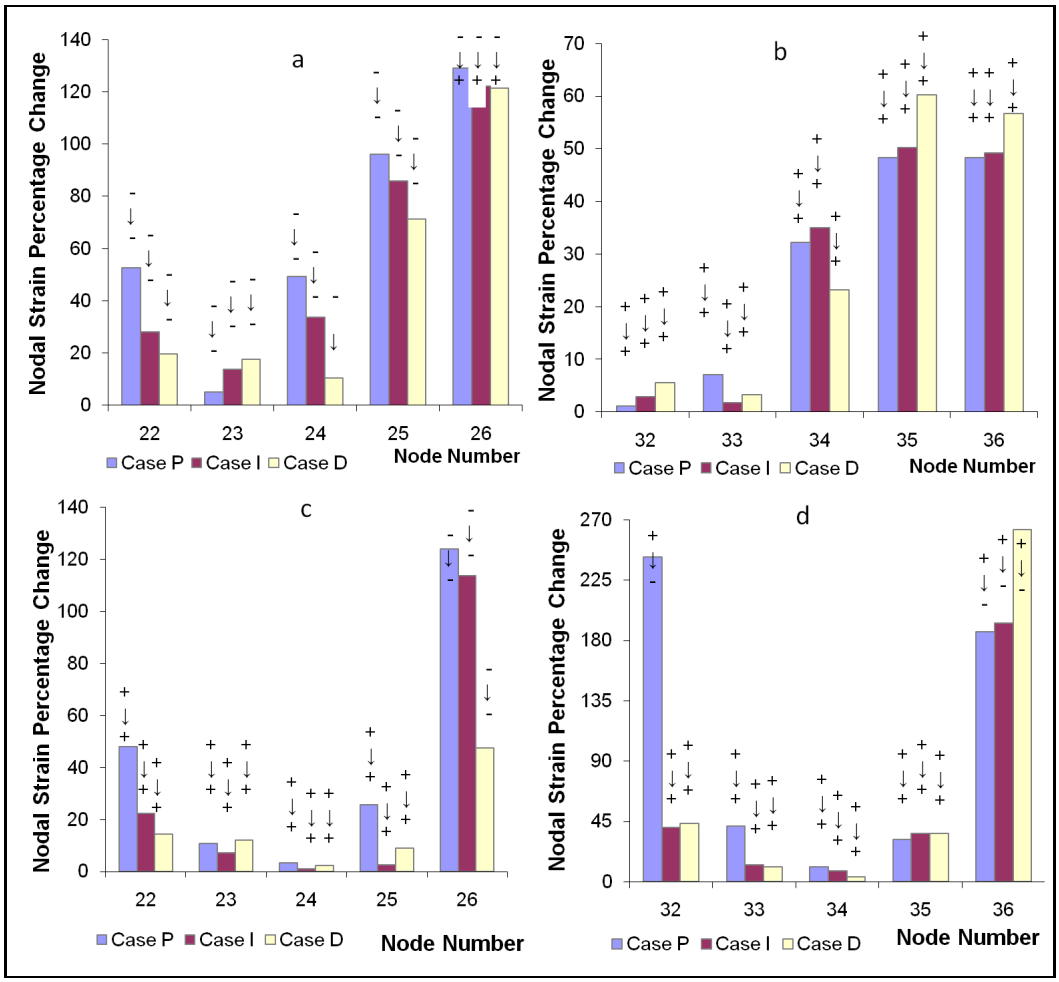

Figure 3.6 (A)Comparison of percentage changes of fiber direction nodal strain values compared to Case no MT for first row. (B)Comparison of percentage changes of fiber direction nodal strain values compared to Case no MT for second row, (C)Comparison of percentage changes of cross-fiber direction nodal strain values compared to Case no MT for first row, (D)Comparison of percentage changes of cross-fiber direction nodal strain values compared to Case no MT for second row.

3.2 Effects of Location and Direction of Multiple Location Loading

3.2.1 Loading in Compression on Passive Muscle Model

A downward displacement value of 0.5625 mm is applied on two nodes simultaneously to account for a multiple compressive load. The passive muscle model was positioned relative to its nonmuscular neighboring structures.

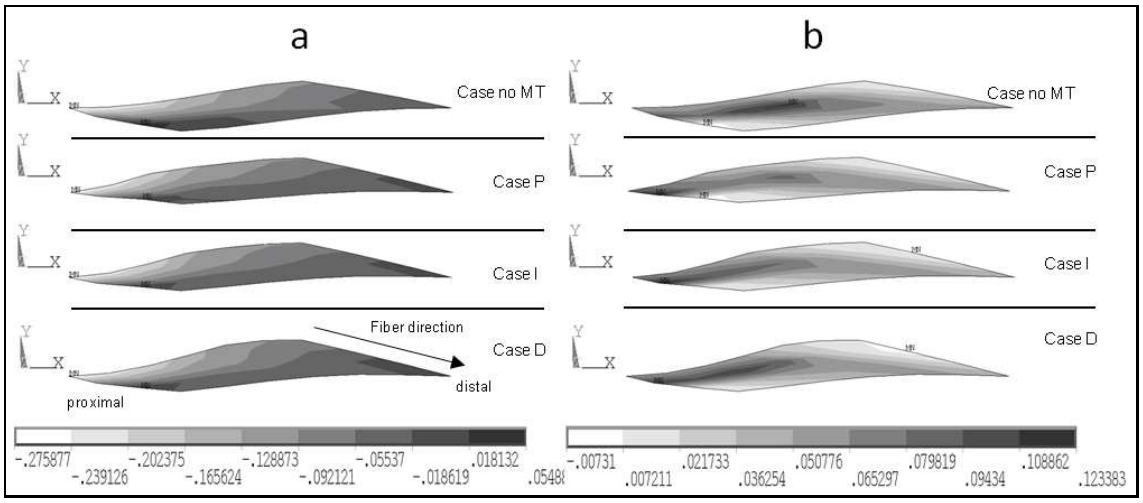

Figure 3.7 (A)Fiber direction strains within modeled active muscle. The muscle is in its initial length and positioned relative to its nonmuscular neighboring structures. Tensioning load is applied towards +y direction. (B)Cross-fiber direction strains within modeled active muscle. The muscle is in its initial length and positioned relative to its nonmuscular neighboring structures.

1. No substantial change of the area of positive strains in fiber direction was seen for Case P-I, and a decrease of the area positive strains was seen for Case I-D compared to Case P (Figure 3.9a). No substantial change was seen on the area of positive strains in cross-fiber direction strain distribution for Case P-I and a decrease of positive strains was seen for Case I-D compared to Case P (Figure 3.9b).

2. In Figure 3.10a and 3.10b, it can be seen that the highest increases (equaling 33 % for first row and 12 % for second row) in percentage change of fiber direction strains are at the most proximal nodes of the rows.

3. Figures 3.10c and 3.10d show that the highest increases (equaling 237 % for first row and 133 % for second row) in percentage change of cross-fiber direction strains are at the most proximal nodes of the rows.

3.2.2 Loading in Compression on Active Muscle Model

A downward displacement value of 0.175 mm was applied on two locations (i.e. Location P and Location I or Location I and Location D (Fig. 1)) simultaneously to

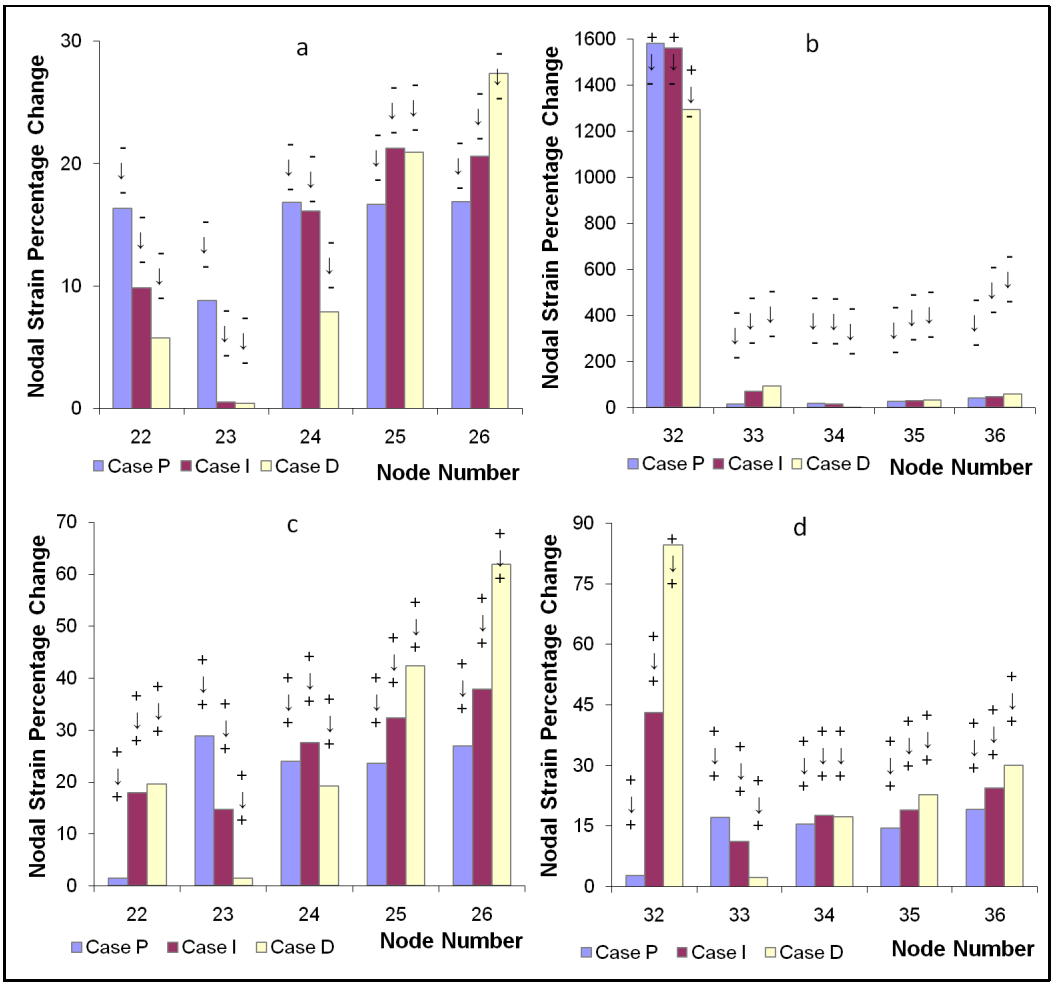

Figure 3.8 (A)Comparison of percentage changes of fiber direction nodal strain values compared to Case no MT for first row. (B)Comparison of percentage changes of fiber direction nodal strain values compared to Case no MT for second row, (C)Comparison of percentage changes of cross-fiber direction nodal strain values compared to Case no MT for first row, (D)Comparison of percentage changes of cross-fiber direction nodal strain values compared to Case no MT for second row.

account for a compressive manual therapy technique. The active muscle model was positioned relative to its nonmuscular neighboring structures.

1. A minor increase of the area of positive strains in fiber direction was seen for Case P-I; on the other hand a decrease of the area positive strains was seen for Case I-D compared to Case P (Figure 3.11a). Also, a minor increase was seen on the area of positive strains in cross-fiber direction strain distribution for Case P-I, and no substantial change was seen in positive strains for Case I-D compared to Case P (Figure 3.11b).

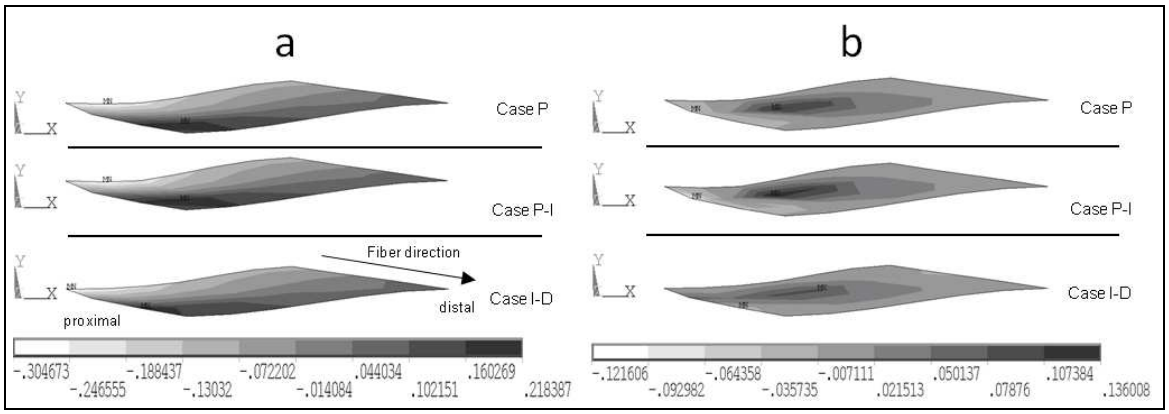

Figure 3.9 (A)Fiber direction strains within modeled passive muscle. The muscle is in its initial length and positioned relative to its nonmuscular neighboring structures. Compressive load is applied towards -y direction. (B)Cross-fiber direction strains within modeled passive muscle. The muscle is in its initial length and positioned relative to its nonmuscular neighboring structures.

2. In Figure 3.12a and 3.12b, it can be seen that the highest increases (equaling 13 % for first row and 110 % for second row) in percentage change of fiber direction strains are at the most proximal nodes of the rows.

3. Figures 3.12c and 3.12d show that the highest increases (equaling 17 % for first row and 2 % for second row) in percentage change of cross-fiber direction strains are at proximal region for first row and distal region for second row.

The value of node 35 in Figure 3.12d was used because the other values changed from a positive value to a less positive value.

3.2.3 Loading in Tension on Passive Muscle Model

An upward displacement value of 0.85 mm was applied on two locations (i.e. Location P and Location I or Location I and Location D (Fig. 1)) simultaneously to account for a compressive manual therapy technique. The passive muscle model was positioned relative to its nonmuscular neighboring structures.

1. No substantial change was seen in the area of positive strains in fiber and cross-

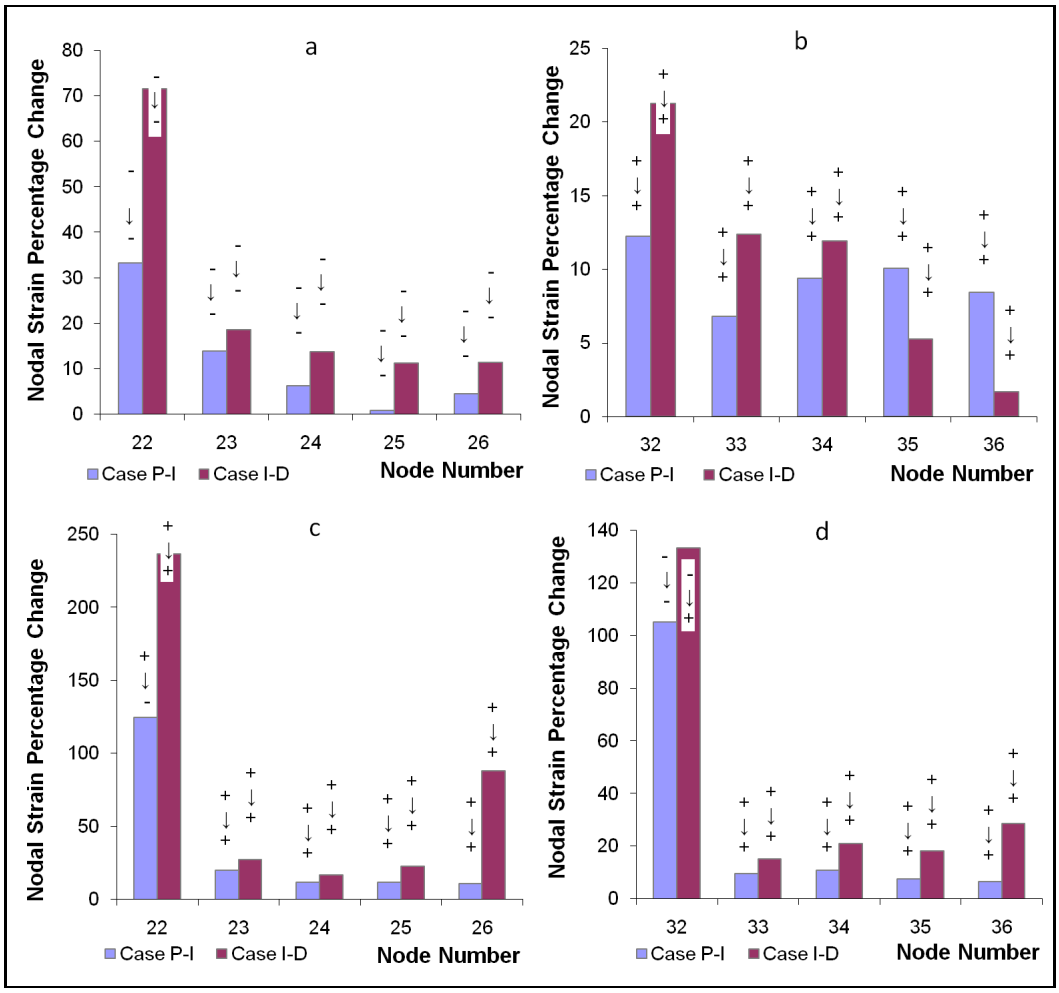

Figure 3.10 (A)Comparison of percentage changes of fiber direction nodal strain values compared to Case no MT for first row. (B)Comparison of percentage changes of fiber direction nodal strain values compared to Case no MT for second row, (C)Comparison of percentage changes of cross-fiber direction nodal strain values compared to Case no MT for first row, (D)Comparison of percentage changes of cross-fiber direction nodal strain values compared to Case no MT for second row.

fiber direction was seen for Case P-I (Figure 3.13a); on the other hand a decrease of the area positive strains in fiber and cross-fiber direction was seen for Case I-D compared to Case P (Figure 3.13b).

2. In Figure 3.14a and 3.14b, it can be seen that the highest increases (equaling 14 % for first row and 3 % for second row) in percentage change of fiber direction strains are at the most proximal nodes of the rows.

3.) Figures 3.14c and 3.14d show that the highest increases (equaling 28 % for first row and 178 % for second row) in percentage change of cross-fiber direction strains are at distal region for first row and proximal region for second row.

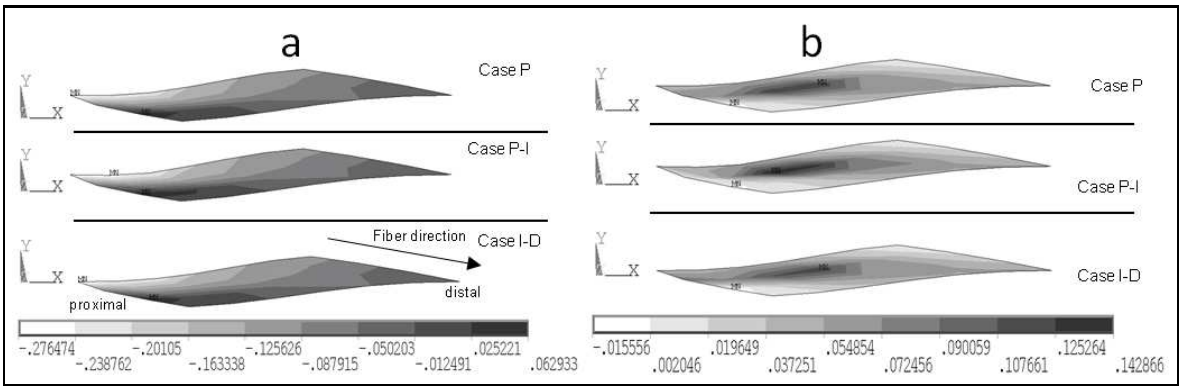

Figure 3.11 (A)Fiber direction strains within modeled active muscle. The muscle is in its initial length and positioned relative to its nonmuscular neighboring structures. Compressive load is applied towards -y direction. (B)Cross-fiber direction strains within modeled active muscle. The muscle is in its initial length and positioned relative to its nonmuscular neighboring structures.

In Figure 3.14a, the value of node 22 was used because the other values either changed from a positive to a negative value or from a negative value to a more negative. Value of node 33 and value of node 23 were used because the others changed from a positive value to a less positive value in Figure 3.14b and 3.14c, respectively. In Figure 3.14d, the value of node 35 was used because the others were not representing the intended effect of manual therapy (i.e. lengthening of muscle)

3.2.4 Loading in Tension on Active Muscle Model

An upward displacement value of 1.0375 mm was applied on two locations (i.e. Location P and Location I or Location I and Location D (Fig. 1)) simultaneously to account for a compressive manual therapy technique. The active muscle model was positioned relative to its nonmuscular neighboring structures.

1. No substantial changes were seen in the area of positive strains in fiber and cross-fiber direction for both Case P-I and Case I-D compared to Case P (Figures 3.15).

2. In Figure 3.16a and 3.16b, it can be seen that the highest increases (equaling 9 % for first row and 22 % for second row) in percentage change of fiber direction

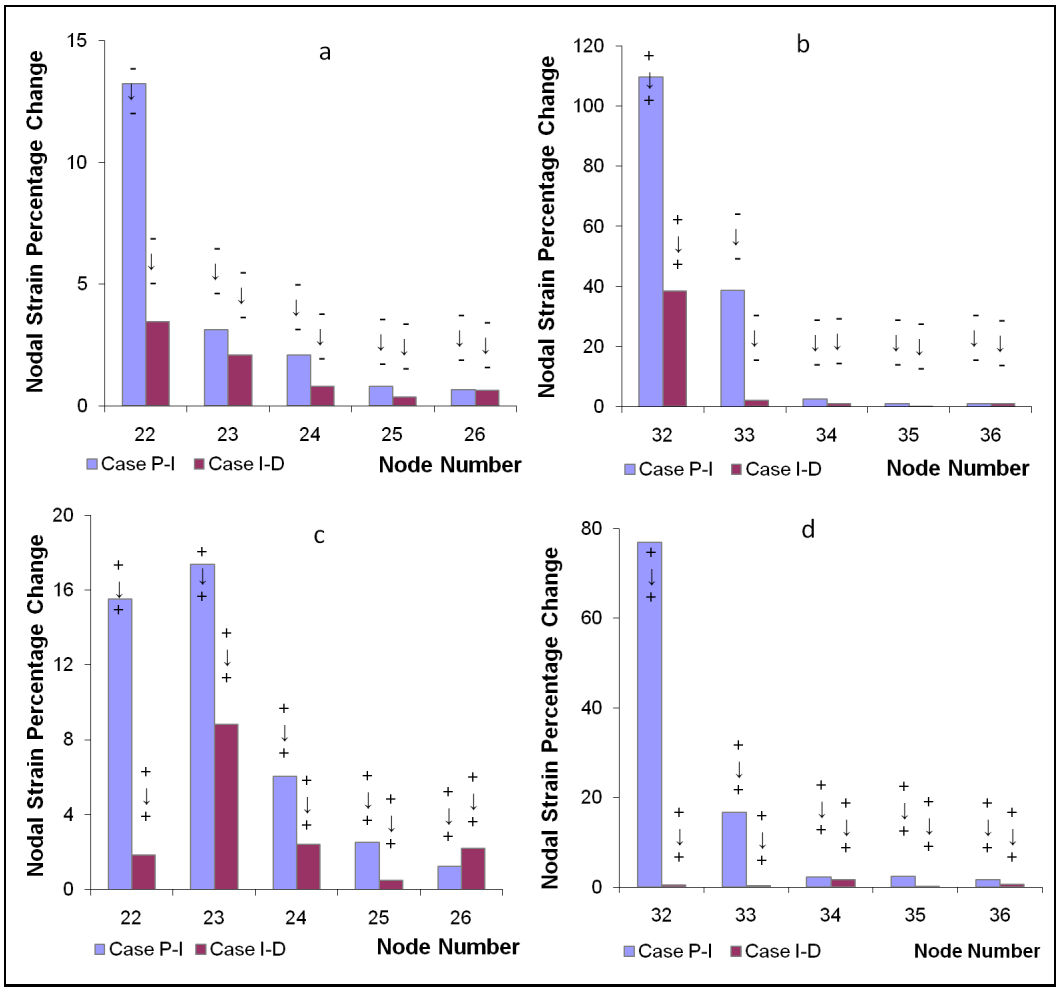

Figure 3.12 (A)Comparison of percentage changes of fiber direction nodal strain values compared to Case no MT for first row. (B)Comparison of percentage changes of fiber direction nodal strain values compared to Case no MT for second row, (C)Comparison of percentage changes of cross-fiber direction nodal strain values compared to Case no MT for first row, (D)Comparison of percentage changes of cross-fiber direction nodal strain values compared to Case no MT for second row.

strains are at the most distal nodes of the rows.

3. Figures 3.16c and 3.16d show that the highest increases (equaling 18 % for first row and 43 % for second row) in percentage change of cross-fiber direction strains are at the most proximal nodes of the rows.

The value of node 33 in Figure 3.16b was not used because it attained a more negative value. In Figure 3.16c, the value of node 22 was taken because the other positive values reduced in amount.

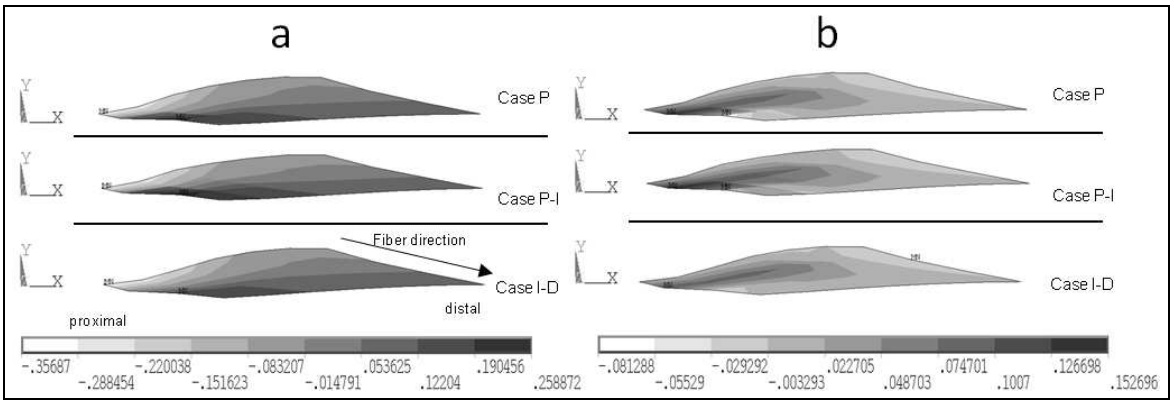

Figure 3.13 (A)Fiber direction strains within modeled passive muscle. The muscle is in its initial length and positioned relative to its nonmuscular neighboring structures. Compressive load is applied towards +y direction. (B)Cross-fiber direction strains within modeled passive muscle. The muscle is in its initial length and positioned relative to its nonmuscular neighboring structures.

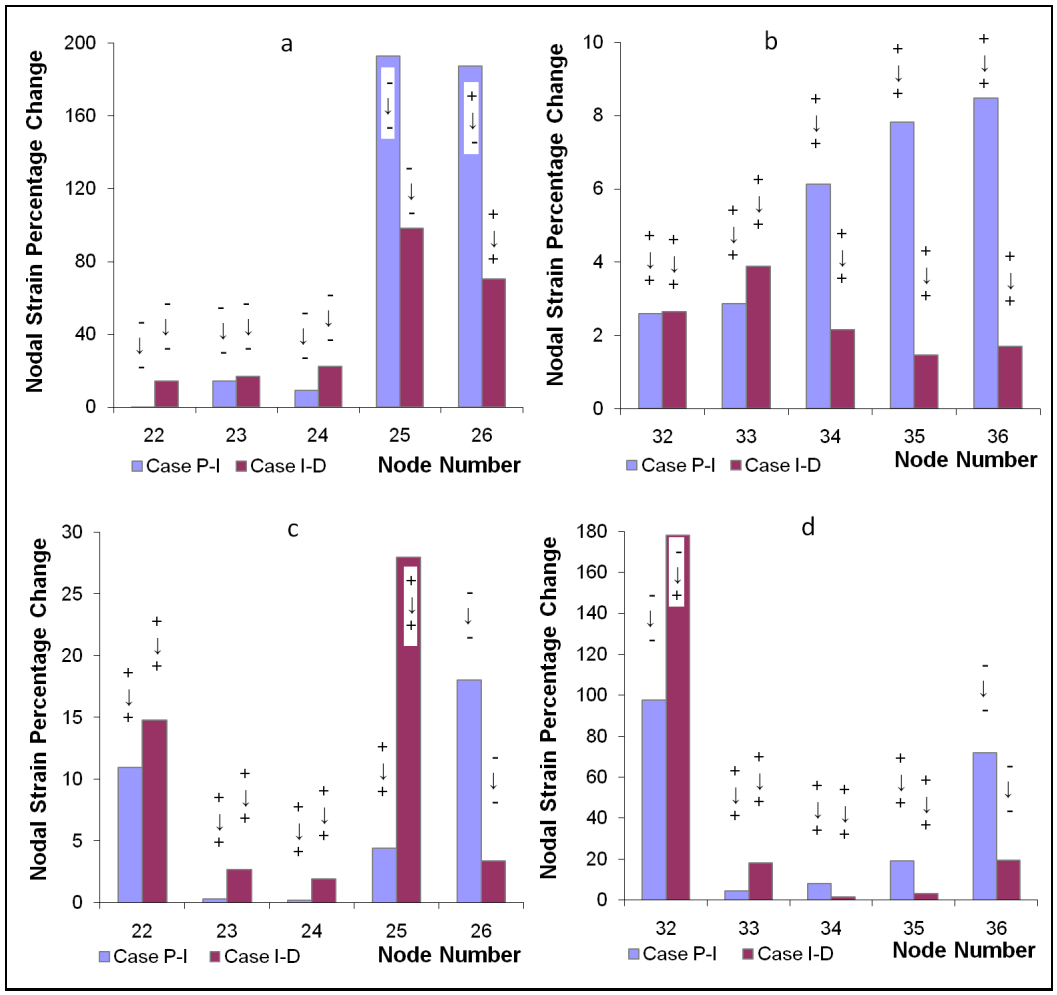

Figure 3.14 (A)Comparison of percentage changes of fiber direction nodal strain values compared to Case no MT for first row. (B)Comparison of percentage changes of fiber direction nodal strain values compared to Case no MT for second row, (C)Comparison of percentage changes of cross-fiber direction nodal strain values compared to Case no MT for first row, (D)Comparison of percentage changes of cross-fiber direction nodal strain values compared to Case no MT for second row.

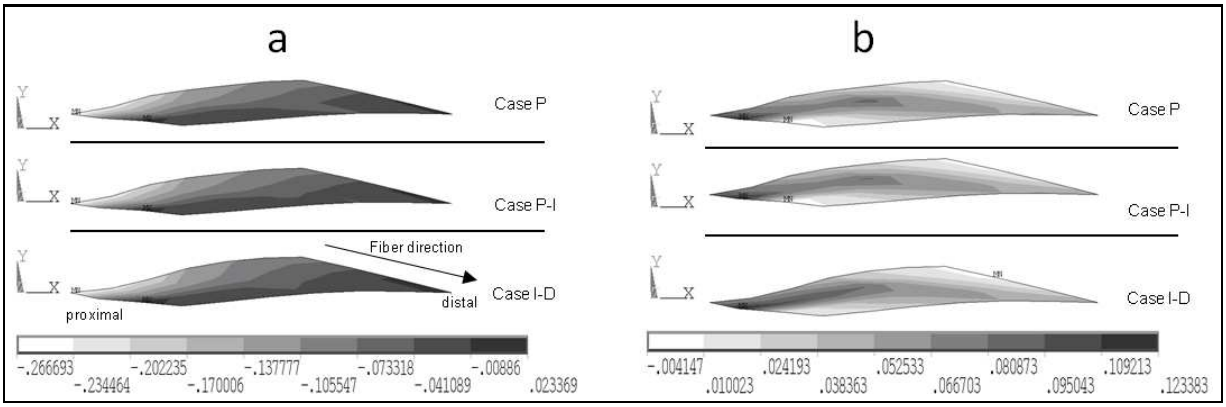

Figure 3.15 (A)Fiber direction strains within modeled active muscle. The muscle is in its initial length and positioned relative to its nonmuscular neighboring structures. Compressive load is applied towards +y direction. (B)Cross-fiber direction strains within modeled active muscle. The muscle is in its initial length and positioned relative to its nonmuscular neighboring structures.

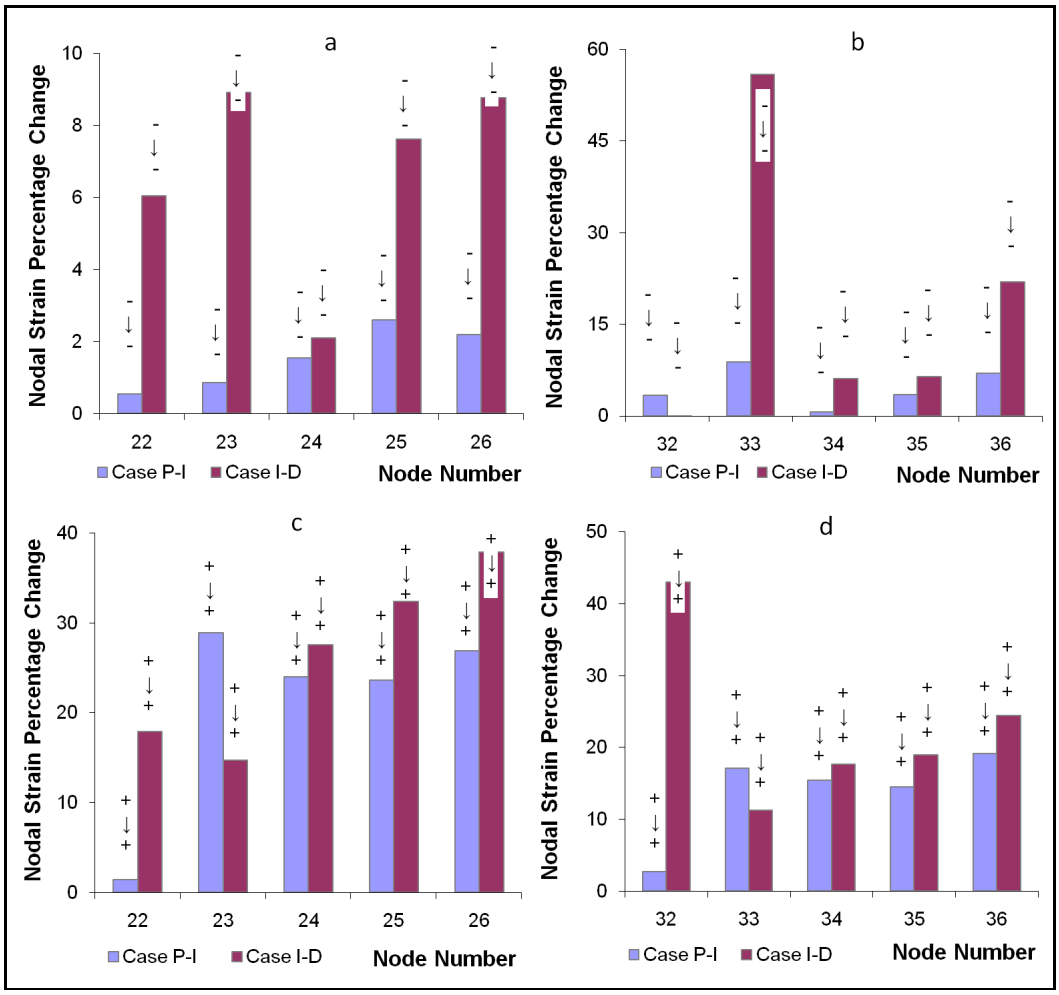

Figure 3.16 (A)Comparison of percentage changes of fiber direction nodal strain values compared to Case no MT for first row. (B)Comparison of percentage changes of fiber direction nodal strain values compared to Case no MT for second row, (C)Comparison of percentage changes of cross-fiber direction nodal strain values compared to Case no MT for first row, (D)Comparison of percentage changes of cross-fiber direction nodal strain values compared to Case no MT for second row.

4. DISCUSSION

4.1 Proximal Location Loading Enhances the Intended Effects of Manual Therapy

4.1.1 Lengthening of Sarcomeres within the Modeled Muscle

Manual therapists generally aim for lengthening of muscle and tendon structures to improve the restricted joint range of motion as a result of the symptoms that cause muscle contractures (e.g. in cerebral palsy, lumbar compartment syndrome). Therefore, in the study, lengthening of sarcomeres within the modeled muscle is the important effect of therapeutic loading.

This study showed that loading the muscle model at a proximal location yields more pronounced percentage changes for both fiber and cross-fiber direction nodal strain. Especially, this effect is more substantial for loading in compression compared to loading in tension. However, for single location loading in tension, maximal percentage change was seen for Case D for fiber direction and also for cross-fiber direction nodal strains (see Figure 3.14).

4.1.2 Improvement in Positive Strains in Sarcomere Length Distributions

Effect of proximal loading on sarcomere length distributions can also be seen in Figures 3.1a, 3.1b, 3.3a, 3.3b, 3.5a and 3.5b, area of positive strains enlarged due to therapeutic loading for Case P. Enlargement of the area of positive strain indicates the enhanced lengthening of sarcomeres compared to Case no MT. In Figure 3.7a and 3.7b, this area narrowed compared to Case no MT for all cases.

4.2 Therapeutic Loading is More Effective in Passive Muscle Model Compared to Activated Muscle Model

4.2.1 Single Location Loading in Compression

As can be seen in Figure3.2 and Figure 3.4, for single location loading in compression causes less increase in percentage changes for active muscle model compared to passive muscle model. In passive case, applied load was increased by 117 % (i.e., 0.65 mm) compared to active case (i.e., 0.3 mm). However, even if we compensate for this applied load difference by increasing the nodal percentage values, therapeutic loading causes more lengthening of sarcomeres in passive case. The dramatic increase for percentage change of fiber direction strain (i.e. 2234 %) for second row was neglected in this comparison (Figure 3.4b).

4.2.2 Single Location Loading in Tension

Single location loading in tension also causes more substantial effect on percentage changes for passive muscle model compared to activated muscle(Figure 3.6 and Figure 3.8). In this case, applied load is even higher for active case (i.e., 1.0375 mm) compared to passive case (i.e., 0.925 mm) .

4.2.3 Multiple Location Loading in Compression

Loading the muscle model compressively at multiple locations yields more increases in percentage changes of nodal strains in passive case compared to the activated muscle model cases (Figure 3.10 and Figure 3.12). In passive case, loading was increased by an amount of 221 %, if the applied loads for active case were revised the increases for fiber direction percentage change of nodal strains became higher for active case.

4.2.4 Multiple Location Loading in Tension

Multiple location loading in tensio also showed a more pronounced increase in percentage changes of nodal strain values for passive case, even though the applied load was less for the passive case than that of active case (Figure 12 and Figure 14).

We conclude that if manual therapists apply the treatment to patient during exercise, the intended effects may be less. As a result, the targeted muscle might be in a passive condition for a more pronounced effect of therapy.

4.3 Increasing the Number of Loading Locations Does not Enhance the Intended Effects of Manual Therapy

The values of displacements of load in tension for single and multiple cases were the same. However, the values of percentage change of fiber and cross-fiber direction strains decreased for the multiple loading case(i.e. from % 27, % 59, % 20, and % 85 to % 9, % 22, % 18, and % 43; respectively fiber direction strain of first row, fiber direction strain of second row, cross-fiber direction strain of first row, cross-fiber direction strain of second row) compared to single load case.

The values of displacements of other loading techniques for single and multiple cases were not the same. However additional loading did not cause pronounced lengthening, when the displacement values of single and multiple loading cases were revised to make them comparable.

4.4 Limitations of the Study

It was reported that there exist some mechanical properties between healthy and contractured muscles [21]. These differences in the mechanical properties of the

modeled EDL muscle and its extracellular connections were neglected to understand the basic principles of the mechanical mechanisms of therapeutic loading.

Another limitation is that the applied loads on the upper and lower layers of the model were subjected to the same amount of load; however when a manual therapist applies a superficial load on the muscle, the lower layer will be less deformed compared to upper layer.

Another important aspect of treatment that was not included in our model is that effects of a particular amount of applied displacement will be different for different body temperatures.

REFERENCES

1. MacIntosh, B. R., P. F. Gardiner, and A. J. McComas, *Skeletal Muscle: Form and Function, 2nd ed.*

2. Silvertborn, D. U., *Human Physiology: An Integrated Approach, 3rd ed.*, Pearson Education Inc., Benjamin Cummings, 2004.

3. Hammer, W. I., "The effect of mechanical load on degenerated soft tissue," *Journal of Bodyworks and Movement Therapies*, Vol. 12, pp. 246–256, 2008.

4. Hammer, W. L., and M. T. Pfefer, "Treatment of a case of subacute lumbar compartment syndrome using the graston technique," *Journal of Manipulative and Physiological Therapeutics*, pp. 199–204, March-April 2005.

5. Yucesoy, C. A., B. H. F. J. M. Koopman, P. A. Huijing, and H. J. Grootenboer, "Three-dimensional finite element modeling of skeletal muscle using a two-domain approach: linked fiber-matrix mesh model," *Journal of Biomechanics*, Vol. 35, pp. 1253–1262, April 2002.

6. Barnes, M. F., "The basic science of myofascial release: morphologic change in connective tissue," *Journal of Bodyworks and Movement Therapies*, Vol. 1, pp. 231–238, July 1997.

7. Threlkeld, A. J., "The effects of manual therapy on connective tissue," *Physical Therapy*, Vol. 72, pp. 893–902, December 1992.

8. Hoeksma, H. L., J. Dekker, H. K. Ronday, A. Heering, N. van der Lubbe, C. Vel, F. C. Breedveld, and C. H. M. van den Ende, "Comparison of manual therapy and exercise therapy in osteoarthritis of the hip: a randomized clinical trial," *Arthritis and Rheumatism (Arthritis Care and Research)*, Vol. 51, pp. 722–729, October 2004.

9. Bell, J., "Massage therapy helps to increase range of motion, decrease pain and assist in healing a client with lowback pain and sciatica symptoms," *Journal of Bodywork and Movement Therapies*, Vol. 12, pp. 281–289, January 2008.

10. Chaundry, H., C. Y. Huang, R. Schleip, Z. Ji, B. Bukiet, and T. Findley, "Viscoelastic behavior of human fasciae under extension in manual therapy," *Journal of Bodyworks and Movement Therapies*, Vol. 11, pp. 159–167, 2007.

11. Chaundry, H., B. Bukiet, and T. Findley, "Mathematical analysis of applied loads on skeletal muscles during manual therapy," *J Am Osteopath Assoc*, Vol. 108, pp. 680–688, 2008.

12. Chiradejnant, A., J. Latimer, and C. G. Maher, "Forces applied during manual therapy to patients with low back pain," *Journal of Manipulative and Physiological Therapeutics*, Vol. 25, no. 6, pp. 362–369, 2007.

13. Bialosky, J. E., M. D. Bishop, D. D. Price, M. E. Robinson, and S. Z. George, "The mechanisms of manual therapy in the treatment of musculoskeletal pain: a comprehensive model," *Manual Therapy*, Vol. 14, pp. 531–538, 2009.

14. Huyghe, J. M., D. H. van Campen, T. Arts, and R. M. Heethaar, "A two-phase finite element model of the diastolic left ventricle," *Journal of Biomechanics*, Vol. 24, pp. 527–538, 1991.

15. Strumpf, R. K., and J. D. H. et al, "Biaxial mechanical properties of passive and tetanized canine diaphragm," *Journal of Biomechanics*, Vol. 265, pp. 469–475, 1993.

16. Zuurbier, C. J., J. W. Heslinga, M. B. L. de Groot, and W. J. V. der Laarse, "Mean sarcomere length-force relationship of rat muscle fiber bundles," *Journal of Biomechanics*, Vol. 28, pp. 83–87, 1995.

17. Trombitas, K., J. P. Jin, and H. Granzier, "The mechanically active domain of titin in cardiac muscle," *Circulation Research*, Vol. 77, pp. 856–861, 1995.

18. Zuurbier, C. J., A. J. Everard, P. V. der Wees, and P. A. Huijing, "Length-force characteristics of the aponeurosis in the passive and active muscle condition and in the isolated condition," *Journal of Biomechanics*, Vol. 27, pp. 445–453, 1994.

19. Yucesoy, C. A., H. J. F. M. Koopman, G. C. Baan, H. J. Grootenboer, and P. A. Huijing, "Extramuscular myofascial force transmission: experiments and finite element modeling," *Arch Physiol Biochem*, Vol. 111, pp. 377–388, 2003.

20. Yucesoy, C. A., H. J. F. M. Koopman, H. J. Grootenboer, and P. A. Huijing, "Finite element modeling of aponeurotomy: Altered intramuscular myofascial force transmission yields complex sarcomere length distributions determining acute effects," *Biomechanics and Modeling in Mechanobiology*, Vol. 6, pp. 227–243, 2007.

21. Booth, C. M., M. J. F. Coritna-Borja, and T. N. Theologis, "Collagen accumulation in muscles of children with cerebral palsy and correlation with severity of spasticity," *Developmental Medicine and Child Neurology*, Vol. 43, pp. 314–320, 2001.